American Institute of Aeronautics and Astronautics

American Astronautical Society

POST-OPTIMALITY EVALUATION AND ANALYSIS OF A FORMATION FLYING PROBLEM VIA A GAUSS PSEUDOSPECTRAL METHOD

Geoffrey T. Huntington, David A. Benson, and Anil V. Rao

AAS/AIAA Astrodynamics Specialists Conference

POST-OPTIMALITY EVALUATION AND ANALYSIS OF A FORMATION FLYING PROBLEM VIA A GAUSS PSEUDOSPECTRAL METHOD

Geoffrey T. Huntington,[*] David A. Benson,[†] and Anil V. Rao[‡]

The post-optimality analysis of a tetrahedral formation flying optimal control problem is considered. In particular, this four-spacecraft orbit insertion problem is transcribed to a nonlinear programming problem (NLP) using a direct method called the Gauss pseudospectral method. The Karush-Kuhn-Tucker (KKT) conditions for this NLP are then derived and are compared to the conditions obtained via a Gauss pseudospectral discretization of the Hamiltonian boundary-value problem (HBVP) that arises from applying the calculus of variations. It is found that the optimal control obtained by solving the NLP is in excellent agreement with the control obtained from the Gauss pseudospectral discretization of the HBVP. The results obtained in this paper demonstrate the accuracy of the Gauss pseudospectral method and illustrate the usefulness of the Gauss pseudospectral method as a means of gaining insight into the structure of optimally controlled systems.

1 INTRODUCTION

As modern optimal control problems become more complex, they often become impossible to solve analytically. Many continuous-time optimal control problems are approximated as finite-dimensional discrete-time problems and then solved numerically. Methods for solving optimal control problems fall into two general categories: indirect methods and direct methods.[1] In an indirect method, extremal trajectories are found by solving a Hamiltonian boundary-value problem (HBVP) derived from the first-order necessary conditions for optimality.[2] The optimal solution is then found by choosing the extremal trajectory with the lowest cost. A benefit of indirect methods is that an accurate co-state is obtained from solving the HBVP, which allows an accurate control to be computed. However, many HBVPs of interest suffer from extreme sensitivity to unknown boundary conditions. Consequently, it is often difficult to obtain a solution to the HBVP, thus making it difficult to use indirect methods to find solutions to optimal control problems. In a direct method, the discrete-time optimal control problem is transcribed to a nonlinear programming problem (NLP) which can then be solved by well developed algorithms. In particular, in a direct method the optimal control problem is transformed to an NLP by discretizing the differential equations at specific time points called *collocation points*.[3] The NLP is then solved using an appropriate numerical optimization algorithm.[4,5]

Direct methods have risen prominence in recent years because it is often easier to solve the NLP than it is to solve the HBVP.[6,7] However, depending on the choice of the discretization of the differential equations, the co-state obtained from many direct methods is significantly

[*]Draper Laboratory Fellow, Guidance and Navigation Division. Ph.D. Candidate, Dept. of Aeronautics and Astronautics, Massachusetts Institute of Technology.

[†]Draper Laboratory Fellow, Guidance and Navigation Division.

[‡]Senior Member of the Technical Staff, Guidance and Navigation Division, Draper Laboratory, 555 Technology Square, Mail Stop 70, Cambridge, MA 02139.

less accurate than the co-state obtained via indirect methods. Consequently, in general, the control obtained from a direct method is less accurate than the control obtained using an indirect method. Well-known software packages employing direct methods include *Optimal Trajectories by Implicit Simulation* (OTIS),[8] *Sparse Optimal Control Software* (SOCS),[9] *Graphical Environment for Simulation and Optimization* (GESOP),[10] *Direct Collocation* (DIRCOL),[11] and *Direct and Indirect Dynamic Optimization* (DIDO).[12]

A relatively new class of direct methods for solving optimal control problems are *pseudospectral methods*.[13-18] In a pseudospectral method, the state and control are approximated using a basis of polynomials.[13] This approximation, in combination with proper choice of the collocation points, leads to an accurate approximation to the solution of the discrete-time optimal control problem. Two pseudospectral methods that have been used in recent years to solve optimal control problems numerically are the *Legendre pseudospectral method*[14,15] and the *Chebyshev pseudospectral method*.[16] In particular, the Legendre pseudospectral method has been applied to a wide variety of applications including atmospheric entry,[19] orbital transfer,[20] trajectory design for a two spacecraft formation,[21] and recently hybrid optimal control.[22]

A recently developed pseudospectral method that has shown promise both in the solution and post-optimality analysis of optimally controlled systems is the *Gauss pseudospectral method*.[23] In the Gauss pseudospectral method, the optimal control problem is discretized at a set of points called *Gauss points*. Unlike previously developed pseudospectral methods,[14-16] in the Gauss pseudospectral method collocation is not performed at the boundary points. This significant difference in collocation has advantages over other pseudospectral methods in that the resulting KKT conditions from the NLP are identical to the discrete form of the first-order optimality conditions where the discrete form is obtained via a Gauss pseudospectral discretization of the continuous-time optimal control problem. As a result, the solution obtained by solving the NLP can be compared directly with the indirect solution found by solving the HBVP. Furthermore, the equivalence between the KKT conditions and the discretized first-order necessary conditions leads to a method for estimating the costates of the continuous-time optimal control problem using the KKT multipliers of the NLP. It is known that the Gauss pseudospectral costate estimate satisfies the discrete form of the costate dynamic relations as well as the costate boundary conditions, resulting in a solution that satisfies the of optimality conditions at the Gauss points. Details of the Gauss pseudospectral method are found in Ref. 23.

In this research, a post-optimality analysis of a tetrahedral formation flying optimal control problem is performed using the Gauss pseudospectral method. For this minimum-fuel configuration problem, four spacecraft must optimally transfer from an initial circular parking orbit to an elliptical terminal reference orbit while satisfying particular formation constraints. Two variations of this trajectory optimization problem are considered. In the first problem the trajectory is terminated upon satisfying the required terminal position constraints. In the second problem the trajectory is extended one full orbit beyond that of the first problem such that the terminal conditions are the same as those attained one period earlier. The resulting optimal solutions have already been presented in a previous work.[24] This work analyzes the accuracy of those optimal solutions. Specifically, the discrete control from the NLP is compared to the control obtained from the first-order optimality conditions of the HBVP, discretized at the Gauss points. In order to make this comparison, a costate mapping principle (for both the Gauss points and the boundary points) is derived. The results obtained in this paper show that the control obtained from the Gauss pseudospectral method is in excellent agreement with the control predicted by the first-order optimality conditions of the continuous-time optimal control problem. Furthermore, the results presented here demonstrate the accuracy and usefulness of the Gauss pseudospectral method as a way of solving complex optimal control problems.

2 CONTINUOUS BOLZA PROBLEM

Consider the following general optimal control problem.[25,26] Determine the state $\mathbf{x}(t) \in \mathbb{R}^n$, control $\mathbf{u}(t) \in \mathbb{R}^m$, and final time t_f, that minimize the Bolza cost functional

$$J = \Phi(\mathbf{x}(t_f), t_f) + \int_{t_o}^{t_f} g(\mathbf{x}(t), \mathbf{u}(t), t) dt \tag{1}$$

subject to the differential dynamic constraints,

$$\dot{\mathbf{x}}(t) = \mathbf{f}(\mathbf{x}(t), \mathbf{u}(t), t), \qquad t \in [t_0, t_f] \tag{2}$$

the boundary conditions

$$\boldsymbol{\phi}(\mathbf{x}(t_o), t_o, \mathbf{x}(t_f), t_f) = \mathbf{0} \tag{3}$$

and equality control constraints enforced as path constraints

$$\mathbf{C}(\mathbf{u}(t), t) = \mathbf{0}, \qquad t \in [t_0, t_f] \tag{4}$$

In Eqs. (1)-(4), the functions Φ, g, f, ϕ, and C are defined as follows:

$$\begin{array}{lll}
\Phi & : & \mathbb{R}^n \times \mathbb{R} \to \mathbb{R} \\
g & : & \mathbb{R}^n \times \mathbb{R}^m \times \mathbb{R} \to \mathbb{R} \\
\mathbf{f} & : & \mathbb{R}^n \times \mathbb{R}^m \times \mathbb{R} \to \mathbb{R}^n \\
\boldsymbol{\phi} & : & \mathbb{R}^n \times \mathbb{R} \times \mathbb{R}^n \times \mathbb{R} \to \mathbb{R}^q \\
\mathbf{C} & : & \mathbb{R}^m \times \mathbb{R} \to \mathbb{R}^c
\end{array} \tag{5}$$

The problem of Eqs. (1)-(4) will be referred to as the continuous Bolza problem. Extremal trajectories of the Bolza problem of Eqs. (1)-(4) can be found by solving a Hamiltonian boundary value problem (HBVP) that results from applying the calculus of variations. First, the Augmented Hamiltonian, $\mathcal{H}$, is defined as

$$\mathcal{H}(\mathbf{x}, \mathbf{u}, \boldsymbol{\lambda}, \boldsymbol{\mu}, t) = g(\mathbf{x}, \mathbf{u}, t) + \boldsymbol{\lambda}^T \mathbf{f}(\mathbf{x}, \mathbf{u}, t) + \boldsymbol{\mu}^T \mathbf{C}(\mathbf{u}, t) \tag{6}$$

where $\mathbf{x} = \mathbf{x}(t)$ and $\mathbf{u} = \mathbf{u}(t)$. Furthermore, the dynamic costate is $\boldsymbol{\lambda} = \boldsymbol{\lambda}(t) \in \mathbb{R}^n$ and control costate is $\boldsymbol{\mu} = \boldsymbol{\mu}(t) \in \mathbb{R}^c$. The resulting HBVP is then given as

$$\frac{d\mathbf{x}}{dt} = \mathbf{f}(\mathbf{x}(t), \mathbf{u}(t), t) = \frac{\partial \mathcal{H}}{\partial \boldsymbol{\lambda}}, \tag{7}$$

$$\frac{d\boldsymbol{\lambda}}{dt} = -\frac{\partial g}{\partial \mathbf{x}} - \boldsymbol{\lambda}^T(t) \frac{\partial \mathbf{f}}{\partial \mathbf{x}} = -\frac{\partial \mathcal{H}}{\partial \mathbf{x}}, \tag{8}$$

$$\mathbf{0} = \frac{\partial g}{\partial \mathbf{u}} + \boldsymbol{\lambda}^T(t) \frac{\partial \mathbf{f}}{\partial \mathbf{u}} + \boldsymbol{\mu}^T(t) \frac{\partial \mathbf{C}}{\partial \mathbf{u}} = \frac{\partial \mathcal{H}}{\partial \mathbf{u}}, \tag{9}$$

$$\mathbf{0} = \boldsymbol{\phi}(\mathbf{x}(t_o), t_o, \mathbf{x}(t_f), t_f), \tag{10}$$

$$\mathbf{0} = \mathbf{C}(\mathbf{u}(t), t), \tag{11}$$

$$\boldsymbol{\lambda}(t_o) = -\boldsymbol{\nu}^T \frac{\partial \boldsymbol{\phi}}{\partial \mathbf{x}(t_o)}, \tag{12}$$

$$\boldsymbol{\lambda}(t_f) = \frac{\partial \Phi}{\partial \mathbf{x}(t_f)} + \boldsymbol{\nu}^T \frac{\partial \boldsymbol{\phi}}{\partial \mathbf{x}(t_f)}, \tag{13}$$

$$\mathcal{H}(t_f) = -\frac{\partial \Phi}{\partial t_f} - \boldsymbol{\nu}^T \frac{\partial \boldsymbol{\phi}}{\partial t_f} \tag{14}$$

$$\tag{15}$$

where $\boldsymbol{\nu} \in \mathbb{R}^q$ are the Lagrange multipliers associated with the boundary conditions.

3 GAUSS PSEUDOSPECTRAL METHOD

The Bolza problem is defined on the time interval $t \in [t_0, t_f]$. However, in order to apply the Gauss pseudospectral method,[23] the time interval $t \in [t_0, t_f]$ must be transformed to the time interval $\tau \in [-1, 1]$. The transformation that maps the interval $t \in [t_0, t_f]$ to $\tau \in [-1, 1]$ is given as

$$\tau = \frac{2t - (t_f + t_0)}{t_f - t_0} \tag{16}$$

Using Eq. (16), the cost functional of Eq. (1) is then given in terms of τ as

$$J = \Phi(\mathbf{x}(1), t_f) + \frac{t_f - t_0}{2} \int_{-1}^{1} g(\mathbf{x}(\tau), \mathbf{u}(\tau), \tau; t_0, t_f) d\tau \tag{17}$$

Similarly, the dynamic constraints of Eq. (2), the boundary conditions of Eq. (3) and control path constraints of Eq. (4) are given in terms of $\tau \in [-1, 1]$ as

$$\frac{2}{t_f - t_0} \frac{d\mathbf{x}}{d\tau} = \mathbf{f}(\mathbf{x}(\tau), \mathbf{u}(\tau), \tau; t_0, t_f), \tag{18}$$

$$\boldsymbol{\phi}(\mathbf{x}(-1), t_0, \mathbf{x}(1), t_f) = \mathbf{0}, \tag{19}$$

$$\mathbf{C}(\mathbf{u}(\tau), \tau; t_0, t_f) = \mathbf{0} \tag{20}$$

The continuous Bolza problem is now discretized pseudospectrally by approximating the state $\mathbf{x}(\tau)$, by a polynomial, $\mathbf{X}(\tau) \in \mathbb{R}^n$. This polynomial approximation is formed using a basis of $N + 1$ Lagrange interpolating polynomials, $L_0(\tau), \ldots, L_N(\tau)$, on the interval from $[-1, 1]$ as

$$\mathbf{x}(\tau) \approx \mathbf{X}(\tau) = \sum_{i=0}^{N} \mathbf{x}(\tau_i) L_i(\tau) \tag{21}$$

where $L_i(\tau)$, $(i = 1, \ldots, n)$ is the ith Lagrange polynomial and is defined as

$$L_i(\tau) = \prod_{j=0, j \neq i}^{N} \frac{(\tau - \tau_j)}{(\tau_i - \tau_j)} \tag{22}$$

It is known that $L_i(\tau)$ has the property that

$$L_i(\tau_j) = \delta_{ij} = \begin{cases} 1 & i = j \\ 0 & i \neq j \end{cases}, \qquad i, j = 0, \ldots, N \tag{23}$$

The interpolation points used here are the initial point, $(\tau_0 = -1)$, along with the N Gauss points where the Gauss points lie on the interior of the interval $[-1, 1]$. The derivative of the state approximation in Eq. (21) is collocated at the N Gauss points as follows:[23]

$$\left[\frac{d\mathbf{x}}{d\tau} \right]_{\tau_k} \approx \left[\frac{d\mathbf{X}}{d\tau} \right]_{\tau_k} = \sum_{i=0}^{N} \mathbf{X}(\tau_i) \left(\frac{dL_i}{d\tau} \right)_{\tau_k} = \sum_{i=0}^{N} D_{ki} \mathbf{X}(\tau_i) = \mathbf{f}(\mathbf{X}(\tau_k), \mathbf{U}(\tau_k), \tau_k), \qquad k = 1 \ldots N \tag{24}$$

where D_{ki} are elements in the $D \in \mathbb{R}^{N \times (N+1)}$ *Differentiation Matrix*. For clarity, this matrix is divided into two submatrices. The first column of D, corresponding to the initial point, τ_0, is isolated and denoted as $\bar{D} \in \mathbb{R}^N$, where $\bar{D}_k = \dot{L}_0(\tau_k)$. The remaining part of D, denoted $\tilde{D} \in \mathbb{R}^{N \times N}$, corresponds to the collocation at the Gauss points. It is known that $\tilde{D}_{ki} = \dot{L}_i(\tau_k)$. The approximation to the derivative of the state at the Gauss points is then given as

$$\left[\frac{d\mathbf{x}}{d\tau} \right]_{\tau_k} = \dot{\mathbf{x}}(\tau_k) \approx \dot{\mathbf{X}}(\tau_k) = \bar{D}_k \mathbf{X}(\tau_0) + \sum_{i=1}^{N} \tilde{D}_{ki} \mathbf{X}(\tau_i), \qquad k = 1 \ldots N \tag{25}$$

The continuous-time optimal control problem is now transcribed to a nonlinear programming problem (NLP) using the variables $\mathbf{X}_k = \mathbf{X}(\tau_k) \in \mathbb{R}^n$ for the state and $\mathbf{U}_k = \mathbf{U}(\tau_k) \in \mathbb{R}^m$ for the control at the kth Gauss point, where $k = 1, \ldots, N$. The initial and final states, $\mathbf{X}_0 = \mathbf{X}(\tau_0) \in \mathbb{R}^n$ and $\mathbf{X}_f = \mathbf{X}(\tau_f) \in \mathbb{R}^n$, respectively, are also included as variables in the NLP, for a total of $N + 2$ *nodes*. Note that when using the Gauss Pseudospectral method, the differential dynamic constraints are applied only at the N collocation points whereas the state is approximated at $N + 1$ interpolation points (including $\tau_0 = -1$). Furthermore, the problem is discretized at $N + 2$ nodes (including $\tau_0 = -1$ and $\tau_f = 1$). See Ref. 23 for more details.

In this NLP, the cost functional in Eq. (17) is approximated using a Gauss quadrature as

$$J = \Phi(\mathbf{X}_f, t_f) + \frac{(t_f - t_0)}{2} \sum_{k=1}^{N} w_k g(\mathbf{X}_k, \mathbf{U}_k, \tau_k; t_0, t_f) \tag{26}$$

where w_k are the Gauss weights. The discretized differential dynamic constraints, boundary constraints, and control path constraints of Eq. (18) (collocated at Gauss points) are given as

$$\bar{D}_k \mathbf{X}_0 + \sum_{i=1}^{N} \tilde{D}_{ki} \mathbf{X}_i = \frac{t_f - t_0}{2} \mathbf{f}(\mathbf{X}_k, \mathbf{U}_k, \tau_k; t_0, t_f), \qquad k = 1, \ldots, N \tag{27}$$

In addition to the dynamic constraints, the initial and final state are related via the quadrature

$$\mathbf{X}_f = \mathbf{X}_0 + \frac{t_f - t_0}{2} \sum_{k=1}^{N} w_k \mathbf{f}(\mathbf{X}_k, \mathbf{U}_k, \tau_k; t_0, t_f) \tag{28}$$

The discretized boundary conditions of Eq. (19) are expressed in their general form as

$$\boldsymbol{\phi}(\mathbf{X}_0, t_0, \mathbf{X}_f, t_f) = \mathbf{0} \tag{29}$$

Lastly, the discretized control path constraints of Eq. (20) are expressed as follows

$$\mathbf{C}(\mathbf{U}_k, \tau_k; t_0, t_f) \leq \mathbf{0}, \qquad k = 1, \ldots, N \tag{30}$$

The cost functional of Eq. (26) together with the constraints of Eqs. (27), (28), (29), and (30) define a nonlinear programming problem (NLP). The solution of this NLP is an approximate solution to the continuous-time optimal control problem.

It is noted that the Gauss pseudospectral method has been extended to problems with multiple phases (see Ref. 23). The extension to a P-phase problem involves repeating the structure for the one-phase formulation P times. Furthermore, the terminal constraints for the first phase, the initial and terminal constraints for the interior phases, and the initial constraints for the Pth phase are replaced by interior point constraints. These interior point constraints include any linkage conditions between adjacent phases and are substituted for Eq. (29) in the above formulation.

$$\begin{aligned} \boldsymbol{\mathcal{L}}_{(0)}^{(1)}(\mathbf{X}_0^{(1)}, t_0^{(1)}) &= \mathbf{0}, \\ \boldsymbol{\mathcal{L}}_{(r)}^{(r+1)}(\mathbf{X}_f^{(r)}, t_f^{(r)}, \mathbf{X}_0^{(r+1)}, t_0^{(r+1)}) &= \mathbf{0}, \\ \boldsymbol{\mathcal{L}}_{(P)}^{(P+1)}(\mathbf{X}_f^{(P)}, t_f^{(P)}) &= \mathbf{0} \end{aligned} \tag{31}$$

where $r = 1, \ldots, P - 1$ phases. In addition to problems with multiple phases, the Gauss pseudospectral method is readily extendible to problems involving multiple vehicles by concatenating the state and control of each spacecraft, thereby forming a single higher dimensional state and control. The optimal control problem can then be posed in the form given above.

4   COSTATE ESTIMATES

We will now derive relationships that map the Lagrange multipliers obtained from the solution of the discrete NLP to the costates of the continuous-time optimal control problem at the Gauss points and the boundary points. The KKT conditions of the NLP are derived by first combining all constraints in the NLP into an augmented cost functional, or Lagrangian:

$$
\begin{aligned}
J_a &= \Phi(\mathbf{X}_f, t_f) + \frac{t_f - t_0}{2} \sum_{k=1}^{N} w_k g(\mathbf{X}_k, \mathbf{U}_k, \tau_k; t_0, t_f) + \boldsymbol{\nu}_r^T \boldsymbol{\mathcal{L}}_{(r)}^{(r+1)} \left(\mathbf{X}_f^{(r)}, t_f^{(r)}, \mathbf{X}_0^{(r+1)}, t_0^{(r+1)} \right) \\
&+ \boldsymbol{\nu}_{r-1}^T \boldsymbol{\mathcal{L}}_{(r-1)}^{(r)} \left(\mathbf{X}_f^{(r-1)}, t_f^{(r-1)}, \mathbf{X}_0^{(r)}, t_0^{(r)} \right) + \frac{t_f - t_0}{2} \sum_{k=1}^{N} w_k \tilde{\boldsymbol{\mu}}_k^T \mathbf{C}(\mathbf{U}_k, \tau_k; t_0, t_f) \\
&+ \sum_{k=1}^{N} \tilde{\boldsymbol{\Lambda}}_k^T \left(\bar{\mathbf{D}}_k \mathbf{X}_0 + \sum_{i=1}^{N} \tilde{\mathbf{D}}_{ki} \mathbf{X}_i - \frac{t_f - t_0}{2} \mathbf{f}(\mathbf{X}_k, \mathbf{U}_k, \tau_k; t_0, t_f) \right) \\
&+ \tilde{\boldsymbol{\Lambda}}_F^T \left(\mathbf{X}_f - \mathbf{X}_0 - \frac{t_f - t_0}{2} \sum_{k=1}^{N} w_k \mathbf{f}(\mathbf{X}_k, \mathbf{U}_k, \tau_k; t_0, t_f) \right)
\end{aligned}
\tag{32}
$$

This formulation uses the multipliers $\boldsymbol{\nu}_r$, $\boldsymbol{\nu}_{r-1}$, $\tilde{\boldsymbol{\mu}}_k$, $\tilde{\boldsymbol{\Lambda}}_k$, and $\tilde{\boldsymbol{\Lambda}}_f$, where $k = 1, \ldots, N$. The KKT conditions are found by setting the gradient of the Lagrangian to zero. First, the partial derivatives of the augmented cost with respect to the control at the Gauss points are given as

$$
\frac{\partial J_a}{\partial \mathbf{U}_k} = \frac{(t_f - t_0) w_k}{2} \frac{\partial g_k}{\partial \mathbf{U}_k} + \frac{(t_f - t_0) w_k}{2} \tilde{\boldsymbol{\mu}}_k^T \frac{\partial \mathbf{C}_k}{\partial \mathbf{U}_k} - \frac{t_f - t_0}{2} \tilde{\boldsymbol{\Lambda}}_k^T \frac{\partial \mathbf{f}_k}{\partial \mathbf{U}_k} - \frac{(t_f - t_0) w_k}{2} \tilde{\boldsymbol{\Lambda}}_F^T \frac{\partial \mathbf{f}_k}{\partial \mathbf{U}_k}
\tag{33}
$$

Multiplying Eq. (33) by $2/(w_k(t_f - t_0))$, $k = 1, \ldots, N$, combining like terms, and setting Eq. (33) to zero results in

$$
\frac{\partial J_a}{\partial \mathbf{U}_k} = \mathbf{0} = \frac{\partial g_k}{\partial \mathbf{U}_k} + \left(-\tilde{\boldsymbol{\Lambda}}_F^T - \frac{\tilde{\boldsymbol{\Lambda}}_k^T}{w_k} \right) \frac{\partial \mathbf{f}_k}{\partial \mathbf{U}_k} + \left(\tilde{\boldsymbol{\mu}}_k^T \right) \frac{\partial \mathbf{C}_k}{\partial \mathbf{U}_k}
\tag{34}
$$

Comparing Eq. (34) to the optimality conditions in Eq. (9), we obtain the following relationships at the Gauss points:

$$
\boldsymbol{\lambda}^T(\tau_k) \approx \boldsymbol{\Lambda}_k^T = -\tilde{\boldsymbol{\Lambda}}_F^T - \frac{\tilde{\boldsymbol{\Lambda}}_k^T}{w_k}, \qquad k = 1, \ldots, N
\tag{35}
$$

$$
\boldsymbol{\mu}^T(\tau_k) \approx \boldsymbol{\mu}_k^T = \tilde{\boldsymbol{\mu}}_k^T, \qquad k = 1, \ldots, N
\tag{36}
$$

Substituting the relationships of Eq. (35) and Eq. (36) into Eq. (34), the KKT condition of Eq. (34) becomes equivalent to the discretized form of the first-order necessary conditions of the HBVP shown in Eq. (9), i.e.

$$
\mathbf{0} = \frac{\partial g_k}{\partial \mathbf{U}_k} + \boldsymbol{\Lambda}_k^T \frac{\partial \mathbf{f}_k}{\partial \mathbf{U}_k} + \boldsymbol{\mu}_k^T \frac{\partial \mathbf{C}_k}{\partial \mathbf{U}_k}
\tag{37}
$$

See Ref. (23) for more details. Furthermore, a costate estimate at the boundary points can be calculated by taking the partial derivative of the augmented cost function with respect to $\mathbf{X}_0$ and $\mathbf{X}_f$. The equations for the costate estimates at the boundaries are then compared to Eq. (12) and Eq. (13) and produce the following mapping relations:

$$
\begin{aligned}
\boldsymbol{\lambda}(\tau_0) &\approx \boldsymbol{\Lambda_0} = \sum_{k=1}^{N} \tilde{\boldsymbol{\Lambda}_k}^T \bar{\mathbf{D}_k} - \tilde{\boldsymbol{\Lambda}_F}^T = -\boldsymbol{\nu}_{r-1}^T \frac{\partial \boldsymbol{\mathcal{L}}_{(r-1)}^{(r)}}{\partial \mathbf{X}(\tau_0)}, \\
\boldsymbol{\lambda}(\tau_f) &\approx \boldsymbol{\Lambda}_f = -\tilde{\boldsymbol{\Lambda}_F}^T = \frac{\partial \Phi}{\partial \mathbf{X}(\tau_f)} - \boldsymbol{\nu}_r^T \frac{\partial \boldsymbol{\mathcal{L}}_{(r)}^{(r+1)}}{\partial \mathbf{X}(\tau_f)}
\end{aligned}
\tag{38}
$$

5 ESTIMATES OF OPTIMAL CONTROL

An estimate of the optimal control at the Gauss points can be found by solving Eq. (37) for $\mathbf{U}_k$, where $k = 1, \ldots, N$. This estimate is then compared to the control obtained by solving the NLP in Section 12. However, in order to obtain the control solution at both the Gauss points and the boundary points $\tau_0 = -1$ and $\tau_f = 1$, the optimal control at the boundaries must be determined. The costate estimates at the boundaries from Eq. (38) make it possible to determine the optimal control at the boundary points by solving a system of equations.[25] The control at the initial time $\tau_0 = -1$ can be found by solving the following system of $c + m$ equations for $\boldsymbol{\mu}_0 \in \mathbb{R}^c$ and $\mathbf{U}_0 \in \mathbb{R}^m$:

$$\left[\frac{\partial g}{\partial \mathbf{U}}\right]_{\tau=\tau_0} + \boldsymbol{\Lambda}_0^T \left[\frac{\partial \mathbf{f}}{\partial \mathbf{U}}\right]_{\tau=\tau_0} - \boldsymbol{\mu}_0^T \left[\frac{\partial \mathbf{C}}{\partial \mathbf{U}}\right]_{\tau=\tau_0} = \mathbf{0},$$
$$\mathbf{C}(\mathbf{U}_0, \tau_0) = \mathbf{0} \tag{39}$$

Similarly, The control at the terminal time $\tau_f = 1$ can be found by solving the following system of $c + m$ equations for $\boldsymbol{\mu}_f \in \mathbb{R}^c$ and $\mathbf{U}_f \in \mathbb{R}^m$:

$$\left[\frac{\partial g}{\partial \mathbf{U}}\right]_{\tau=\tau_f} + \boldsymbol{\Lambda}_f^T \left[\frac{\partial \mathbf{f}}{\partial \mathbf{U}}\right]_{\tau=\tau_f} - \boldsymbol{\mu}_f^T \left[\frac{\partial \mathbf{C}}{\partial \mathbf{U}}\right]_{\tau=\tau_f} = \mathbf{0},$$
$$\mathbf{C}(\mathbf{U}_f, \tau_f) = \mathbf{0} \tag{40}$$

Finally, the optimal control, $\mathbf{U}(\tau)$, is transformed back to the original time domain, $t \in [t_0, t_f]$, by the transformation

$$t = \frac{(t_f - t_0)\tau + (t_f + t_0)}{2} \tag{41}$$

The purpose of the remainder of this paper is to compare the optimal control derived from the multipliers of the NLP (above) with the actual control outputted from the NLP in the context of a spacecraft formation flying application.

6 SPACECRAFT FORMATION CONFIGURATION PROBLEM

Consider the problem of configuring a fleet of four spacecraft via orbital transfer from an initial parking orbit to a terminal reference orbit where the formation attains a desired tetrahedral shape at a specified point in the terminal reference orbit. Assuming that the four spacecraft are deployed simultaneously from the same launch vehicle or upper stage, each spacecraft starts at the same point on a circular orbit of altitude $h_0 = 600$ km and inclination $i_0 = 28$ deg. The desired terminal reference orbit is of size 600 km by 7000 km altitude with an inclination of 28 deg. In addition, at apogee of the terminal reference orbit the formation must be within 10 percent of a regular tetrahedron whose side-length is 10 km.

7 TRAJECTORY EVENT SEQUENCE

In this paper, we consider the following two trajectory configuration problems. The first problem, called the basic problem, terminates upon meeting the required tetrahedral position constraints the first time that the apogee of the reference orbit is attained. The second problem, called the extended problem, extends the first problem by one full orbit such that the terminal conditions attained upon reaching the second apogee are the same as those attained upon reaching the first apogee.

7.1 Trajectory Event Sequence for Basic Configuration Problem

The trajectory event sequence for the basic problem is given as follows. First, the trajectory is divided into four phases with the following sequence: coast, burn, coast, and burn. During the coast phases, it is assumed that the thrust is zero while during the burn phases it is assumed that the thrust is constant at its maximum value $T_{\max}$. Furthermore, at each phase interface it is assumed that the equinoctial elements and the mass are continuous, but that the control is discontinuous. Finally, the initial and terminal times of each phases are free (with the exception, of course, of the first phase where the initial time is fixed to zero). Fig. 1 shows a schematic of the basic configuration problem.
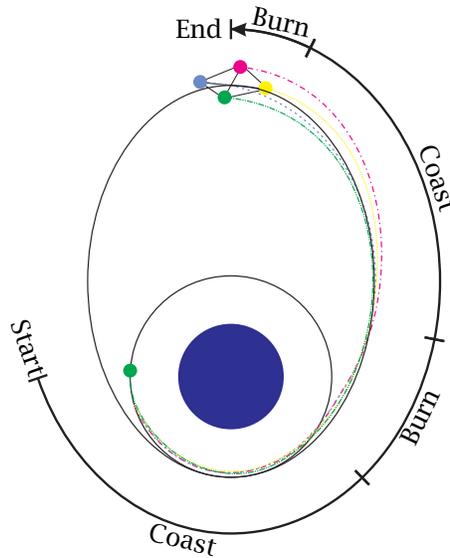
Figure 1: Schematic of Basic Configuration Problem.

7.2 Trajectory Event Sequence for Extended Configuration Problem

The trajectory event sequence for the extended problem is given as follows. First, the trajectory is divided into nine phases with the following sequence. The first four phases are the same at those of the basic problem while the remaining five phases have the following sequence: coast, burn, coast, burn, and coast. Furthermore, all of the assumptions during both the coast and burn phases are the same as those from the basic problem. Finally, all continuity conditions at the phase interfaces are the same as those from the basic problem. Fig. 2 shows a schematic of the basic configuration problem.
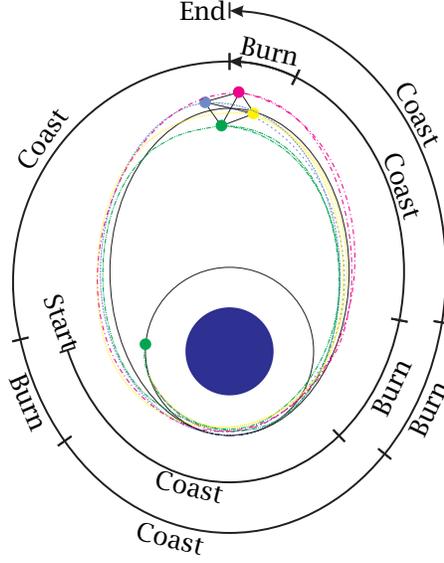
Figure 2: Schematic of Extended Configuration Problem.

8 EQUATIONS OF MOTION AND SPACECRAFT MODEL

8.1 Equations of Motion

The three degree-of-freedom equations of motion for a spacecraft moving over a spherical nonrotating Earth are given in modified equinoctial elements as[27]

$$
\begin{aligned}
\dot{p} &= \frac{2p}{w}\sqrt{\frac{p}{\mu}}a_\theta \\
\dot{P_1} &= \sqrt{\frac{p}{\mu}}\left\{-a_r\cos L + [(w+1)\sin L + P_1]\frac{a_\theta}{w} + [Q_2\sin L - Q_1\cos L]\frac{P_2 a_z}{w}\right\} \\
\dot{P_2} &= \sqrt{\frac{p}{\mu}}\left\{a_r\sin L + [(w+1)\cos L + P_2]\frac{a_\theta}{w} - [Q_2\sin(L) - Q_1\cos L]\frac{P_1 a_z}{w}\right\} \\
\dot{Q_1} &= \sqrt{\frac{p}{\mu}}\left(\frac{s^2}{2w}\right)a_z\sin L \\
\dot{Q_2} &= \sqrt{\frac{p}{\mu}}\left(\frac{s^2}{2w}\right)a_z\cos L \\
\dot{L} &= \sqrt{\mu p}\left(\frac{w}{p}\right)^2 + \sqrt{\frac{p}{\mu}}\frac{Q_2\sin L - Q_1\cos L}{w}a_z
\end{aligned}
\tag{42}
$$

where p is the semi-latus rectum, P_1, P_2, Q_1, and Q_2 have no defined geometric representation, and L is true longitude. Furthermore, in the above equation, $w = p/r = 1 + P_1\sin L + P_2\cos L$, $s^2 = 1 + Q_1^2 + Q_2^2$, and a_r, a_θ, and a_z are the perturbing accelerations in the directions of $\mathbf{e}_r$, $\mathbf{e}_\theta$, and $\mathbf{e}_z$ where $\mathbf{e}_r$ is the unit vector in the radial direction, $\mathbf{e}_z$ is the unit vector in the direction normal to the orbital plane, and $\mathbf{e}_\theta = \mathbf{e}_z \times \mathbf{e}_r$ (thereby completing the right-handed system $\{\mathbf{e}_r, \mathbf{e}_\theta, \mathbf{e}_z\}$). For the application under consideration here, the perturbing accelerations

9

are due entirely to thrust and can be written as

$$
\begin{aligned}
a_r &= \frac{T}{m} u_r \\
a_\theta &= \frac{T}{m} u_\theta \\
a_z &= \frac{T}{m} u_z
\end{aligned}
\tag{43}
$$

where T is the thrust magnitude, m is the spacecraft mass, and u_r, u_θ, and u_z are the $\mathbf{e}_r$, $\mathbf{e}_\theta$, and $\mathbf{e}_z$ components, respectively, of the thrust direction. Finally, the mass flow rate of the engine is governed by the equation

$$
\dot{m} = -\frac{T}{g_0 I_{sp}}
\tag{44}
$$

where g_0 is the sea level acceleration due to gravity and I_{sp} is the specific impulse of the engine.

8.2 Spacecraft Model

In this application we consider four identical spacecraft each with a dry mass of 200 kg and a fuel mass of 300 kg. Furthermore, the maximum thrust level of the engine is 7.015 kN with an engine specific impulse of 287.5 s. It is noted that these physical parameters are typical of a standard apogee kick motor.[28] Finally, all thrusting maneuvers are assumed to be non-impulsive.

9 CONSTRAINTS

9.1 Initial Conditions

All four spacecraft start in the same circular orbit at time $t = 0$. The initial conditions corresponding to this orbit are given in orbital elements as

$$
\begin{array}{llll}
a(0) &= R_e + h_0 \;, & e(0) &= 0 \\
i(0) &= 28 \text{ deg} \;, & \omega(0) &= 270 \text{ deg} \\
\Omega(0) &= 0 \;, & \nu(0) &= 270 \text{ deg}
\end{array}
\tag{45}
$$

where a is the semi-major axis, e is the eccentricity, i is the inclination, ω is the argument of perigee, Ω is the longitude of the ascending node, ν is the true anomaly, R_e is the radius of the Earth, and $h_0 = 600$ km is the initial altitude. It is noted that the initial argument of perigee, $\omega(0)$, is chosen to be the same as that of the terminal reference orbit while the initial true anomaly, $\nu(0)$, is arbitrary. The orbital elements in Eq. (45) are then converted to modified equinoctial elements using a transformation T_{o2e} (see for example Ref. 27) to obtain the initial state in modified equinoctial elements as

$$
\begin{aligned}
p^{(i)}(t_0) &= p_0 \\
P_1^{(i)}(t_0) &= P_{1,0} \\
P_2^{(i)}(t_0) &= P_{2,0} \\
Q_1^{(i)}(t_0) &= Q_{1,0} \\
Q_2^{(i)}(t_0) &= Q_{2,0} \\
L^{(i)}(t_0) &= L_0
\end{aligned}
\quad , \qquad i = 1, \ldots, 4
\tag{46}
$$

where i is the ith spacecraft. Furthermore, the initial mass of each spacecraft is equal to its maximum value, i.e.

$$
m^{(i)}(t_0) = m_{\max}, \qquad i = 1, \ldots, 4
\tag{47}
$$

where for this problem $m_{\max} = 500$ kg.

9.2 Interior Point Constraints

As stated earlier, in order for the trajectory to be continuous at each phase interface, it is necessary to enforce linkage conditions at every phase boundary. These linkage conditions are enforced on the modified equinoctial elements, mass, and time and are given as follows:

$$
\begin{aligned}
p^{(i)}(t_f^{(j)}) &= p^{(i)}(t_0^{(j+1)}) \\
P_1^{(i)}(t_f^{(j)}) &= P_1^{(i)}(t_0^{(j+1)}) \\
P_2^{(i)}(t_f^{(j)}) &= P_2^{(i)}(t_0^{(j+1)}) \\
Q_1^{(i)}(t_f^{(j)}) &= Q_1^{(i)}(t_0^{(j+1)}) \\
Q_2^{(i)}(t_f^{(j)}) &= Q_2^{(i)}(t_0^{(j+1)}) \\
L^{(i)}(t_f^{(j)}) &= L^{(i)}(t_0^{(j+1)}) \\
m^{(i)}(t_f^{(j)}) &= m^{(i)}(t_0^{(j+1)}) \\
t_f^{(i)\,(j)} &= t_0^{(i)\,(j+1)}
\end{aligned}
\qquad
\begin{aligned}
& i = 1,\ldots,4 \\
& j = 1,\ldots,P-1
\end{aligned}
\tag{48}
$$

where i is the ith spacecraft, j is the jth phase and P is the number of phases in the problem under consideration (in this case $P = 4$ for the basic problem and $P = 9$ for the extended problem). Finally, in order to ensure that time is increasing during the trajectory, the following inequality constraints are placed on the time during each phase of the trajectory:

$$
t_f^{(i)\,(j)} = t_0^{(i)\,(j)} \geq 0, \qquad i = 1,\ldots,4 \,,\, j = 1,\ldots,P
\tag{49}
$$

9.3 Path Constraints

During flight, the following two path constraints are imposed on the four spacecraft. First, during the thrust phases of the trajectory it is necessary to constrain the thrust direction to be unit length. Defining the thrust direction as $\mathbf{u}_T = \begin{bmatrix} u_r & u_\theta & u_z \end{bmatrix}^T$, the following constraint is imposed on $\mathbf{u}_T$ during the thrust phases:

$$
\mathbf{u}_T \cdot \mathbf{u}_T = 1
\tag{50}
$$

Second, during flight the mass of each spacecraft cannot fall below the vehicle dry mass. Defining the dry mass of each vehicle as m_{dry}, the following inequality constraint is imposed on the mass of each spacecraft during the each phase of the trajectory:

$$
m^{(i)} \geq m_{\text{dry}}, \qquad i = 1,\ldots,4
\tag{51}
$$

9.4 Terminal Constraints for Basic Problem

The position of the *mesocenter* of the formation is defined as

$$
\bar{\mathbf{r}} = \frac{1}{4} \sum_{i=1}^{4} \mathbf{r}^{(i)}
\tag{52}
$$

where $\mathbf{r}^{(i)}$, $i = 1,\ldots,4$ are the positions of the four spacecraft as measured from the center of the Earth. The first constraint imposed on the formation at $t = t_f$ is that the mesocenter be

located at the apogee of the reference orbit. Defining the position of the apogee of the reference orbit as $\mathbf{r}_a$, the constraint imposed on the position of the mesocenter of the formation at $t = t_f$ is given as

$$\bar{\mathbf{r}}(t_f) = \mathbf{r}_a \tag{53}$$

Next, let r_{rel} be the distance between a vertex of the desired regular tetrahedron and its mesocenter with a side length l. Then the square of the relative distance between each spacecraft and the mesocenter of the formation is constrained to be within 10 percent of r_{rel}^2 at $t = t_f$, i.e.

$$0.9 r_{\mathrm{rel}}^2 \quad \leq \quad (\mathbf{r}^{(i)}(t_f) - \mathbf{r}_a) \cdot (\mathbf{r}^{(i)}(t_f) - \mathbf{r}_a) \quad \leq \quad 1.1 r_{rel}^2, \qquad i = 1, \dots, 4 \tag{54}$$

Third, the volume of the tetrahedron is constrained to be within 10 percent of the ideal volume of the desired regular tetrahedron at $t = t_f$, i.e.

$$0.9 V_I \quad \leq \quad V(t_f) \quad \leq \quad 1.1 V_I \tag{55}$$

where V_I is the volume of the ideal desired regular tetrahedron and V is the volume of the formation where the volume of a tetrahedron is given as

$$V \quad = \quad \frac{8}{3} \sqrt{|\mathbf{R}|} \tag{56}$$

$$\mathbf{R} \quad = \quad \frac{1}{4} \sum_{i=1}^{4} (\mathbf{r}^{(i)} - \bar{\mathbf{r}}) \otimes (\mathbf{r}^{(i)} - \bar{\mathbf{r}})$$

$|\mathbf{R}|$ is the determinant of the volumetric tensor, $\mathbf{R}$, and $\otimes$ is the tensor product between vectors. It is noted that the volume of a regular tetrahedron with side length l is given as

$$V_I = \frac{l^3 \sqrt{2}}{12} \tag{57}$$

Finally, it is required that the trajectories of all four spacecraft terminate at the same time, i.e.

$$t_f^{(1)\,(P)} = t_f^{(2)\,(P)} = t_f^{(3)\,(P)} = t_f^{(4)\,(P)} \tag{58}$$

where t_f is *free*.

9.5 Terminal Constraints for Extended Problem

In addition to the terminal constraints for the basic problem, the terminal constraints for the extended problem include a set of equality constraints that force the first five modified equinoctial elements at the end of phase 4 to equal the first five modified equinoctial elements at the end of phase 9. These equality constraints are given as

$$\begin{aligned}
p^{(i)}(t_f^{(4)}) &= p^{(i)}(t_f^{(9)}) \\
P_1^{(i)}(t_f^{(4)}) &= P_1^{(i)}(t_f^{(9)}) \\
P_2^{(i)}(t_f^{(4)}) &= P_2^{(i)}(t_f^{(9)}) \quad , \qquad i = 1, \dots, 4 \\
Q_1^{(i)}(t_f^{(4)}) &= Q_1^{(i)}(t_f^{(9)}) \\
Q_2^{(i)}(t_f^{(4)}) &= Q_2^{(i)}(t_f^{(9)})
\end{aligned} \tag{59}$$

In addition, in order for the spacecraft to return to the same location one full revolution after achieving the first apogee of the transfer orbit, it is necessary for the true longitude of each

spacecraft at the end of phase 9 to be 2π greater than the true longitude of each spacecraft at the end of phase 4, i.e.

$$L^{(i)}(t_f^{(4)}) + 2\pi = L^{(i)}(t_f^{(9)}), \qquad i = 1, \ldots, 4 \tag{60}$$

Finally, the terminal times of each spacecraft in phase 4 must be equal to one another, i.e.

$$t_f^{(1)\,(4)} = t_f^{(2)\,(4)} = t_f^{(3)\,(4)} = t_f^{(4)\,(4)} \tag{61}$$

10 OPTIMAL CONTROL SPACECRAFT CONFIGURATION PROBLEM

The optimal control spacecraft configuration problem is now stated formally. Using the aforementioned trajectory event sequence, determine the thrust profile that maximizes the sum of the terminal masses of each spacecraft, i.e. maximize the objective functional

$$J = \sum_{i=1}^{4} m^{(i)}(t_f) \tag{62}$$

subject to the differential equation constraints of Eq. (42) and Eq. (44), the initial constraints of Eq. (46) and Eq. (47), the interior point constraints of Eq. (48) and Eq. (49), the path constraints of Eq. (50) and Eq. (51), and the terminal constraints of *either* Eq. (53), Eq. (54) Eq. (55), and Eq. (58) for the basic problem *or* the terminal constraints of Eq. (53), Eq. (54) Eq. (55), Eq. (58), Eq. (59), Eq. (60), and Eq. (61) for the extended problem.

11 NUMERICAL SOLUTION VIA GAUSS PSEUDOSPECTRAL METHOD

The spacecraft configuration problem as described in section 6 - section 10 is solved using the aforementioned Gauss pseudospectral method of Ref. 23. The optimization was carried out with the MATLAB mex interface of the NLP solver SNOPT[29] using analytic first-order derivatives for the constraint Jacobian and the gradient of the objective function. In all cases the optimal control problem was scaled from SI units to an alternate set of units using a length scale of the radius of the Earth and a time scale of one Schuler period. All other quantities were scaled to maintain a canonical transformation. Furthermore, it is important to note that the values of tetrahedral volume in this scaled set of units are extremely small as compared to the norm of the gradient of the volume. Consequently, in order to properly scale the volume and its derivatives, the terminal constraint of Eq. (55) was implemented in the basic problem by taking the 20th root of the volume, i.e. in the basic problem Eq. (55) was implemented as

$$[0.9V_I]^{1/20} \quad \leq \quad \left[V(t_f)\right]^{1/20} \quad \leq \quad [1.1V_I]^{1/20} \tag{63}$$

Similarly, the terminal constraint of Eq. (55) was implemented in the extended problem by taking the 25th root of the volume, i.e. in the extended problem Eq. (55) was implemented as

$$[0.9V_I]^{1/25} \quad \leq \quad \left[V(t_f)\right]^{1/25} \quad \leq \quad [1.1V_I]^{1/25} \tag{64}$$

Finally, for both the basic and extended configuration problem, the optimization was carried out using 15 nodes (i.e. 13 Gauss points) for the thrust phases and 60 nodes (i.e. 58 Gauss points) for the coast phases.

12 RESULTS

The results in this paper focus primarily on the comparison between the control obtained by solving the NLP and the control obtained from the first-order optimality conditions of the discretized HBVP. A separate analysis of the structure of the optimal trajectories for these two problems can be found in Ref. (24).

12.1 Results for Basic Problem

The basic problem was formulated to allow two thrust phases and two coast phases. However, in the optimal solution the second burn phase was of zero duration. Because no control exits during the coast phases, we can examine the entire control profile by looking at the control in the first burn phase. Figs. 3-5 show the optimal control profile during this burn phase for each component of control. The four arcs in each Figure represent the four spacecraft. Furthermore, it can be seen that the control from the NLP matches well with the estimated optimal control derived from the first-order optimality conditions of the HBVP.
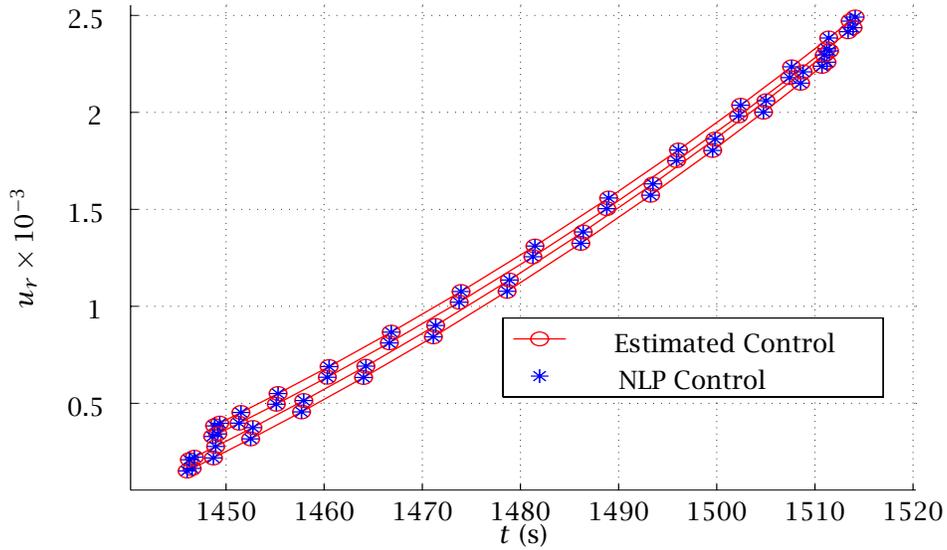
Figure 3: Radial Control Trajectory for Phase 2 of the Basic Configuration Problem.
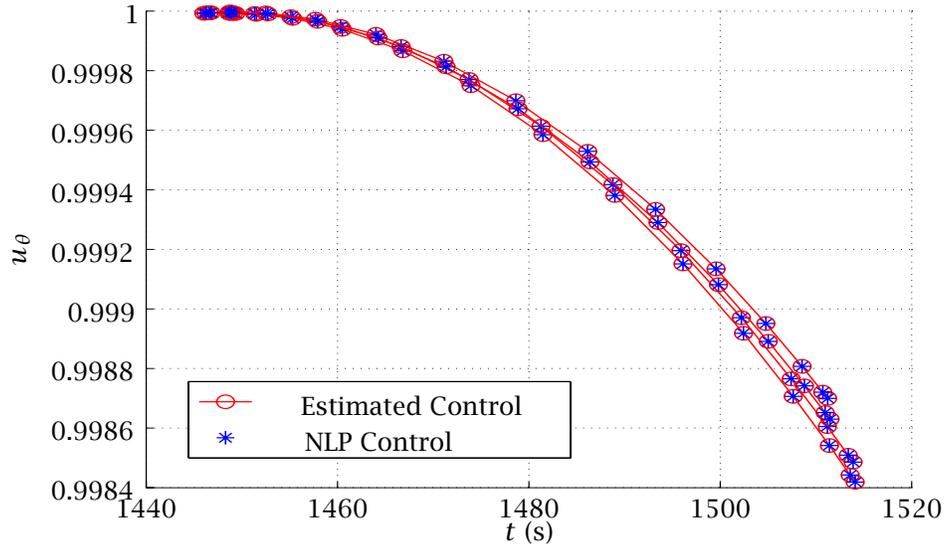
Figure 4: Transverse Control Trajectory for Phase 2 of the Basic Configuration Problem.
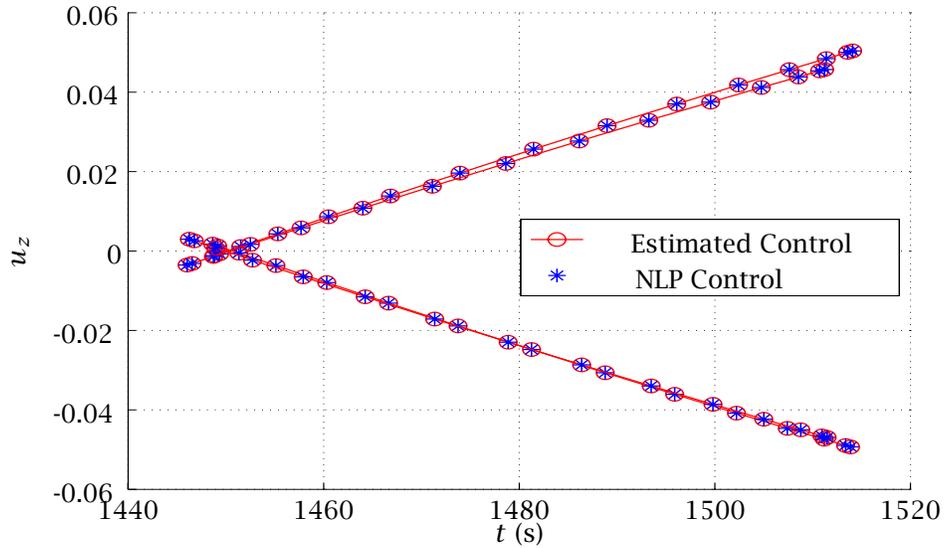
Figure 5: Normal Control Trajectory for Phase 2 of the Basic Configuration Problem.

Figs. 6-8 show the errors in the three components of control, Δu_r, Δu_θ, and Δu_z, between the NLP control solution and the optimal control derived from the calculus of variations. In each component, the maximum error is to the order 10^{-5}. This error can potentially be further reduced by increasing the number of Gauss points chosen in the discretization.
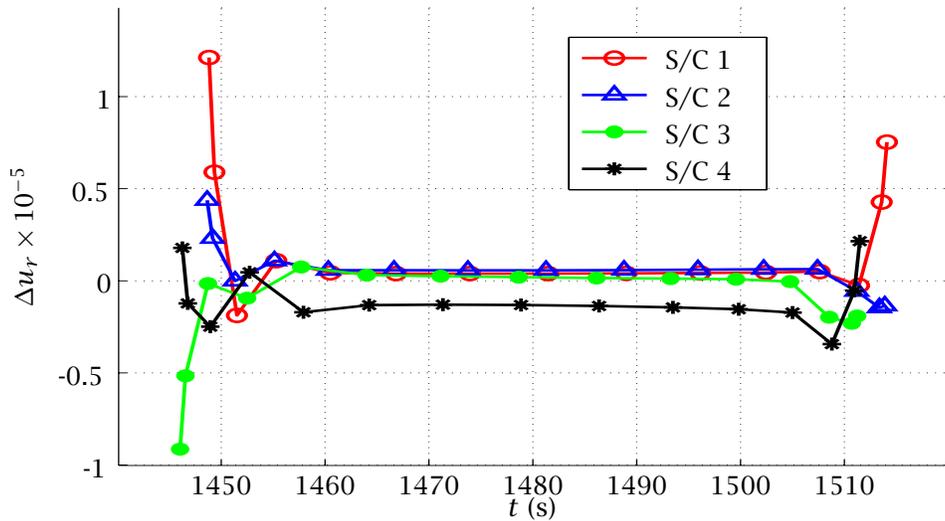

Figure 6: Radial Error in Control for Phase 2 of the Basic Configuration Problem.

15
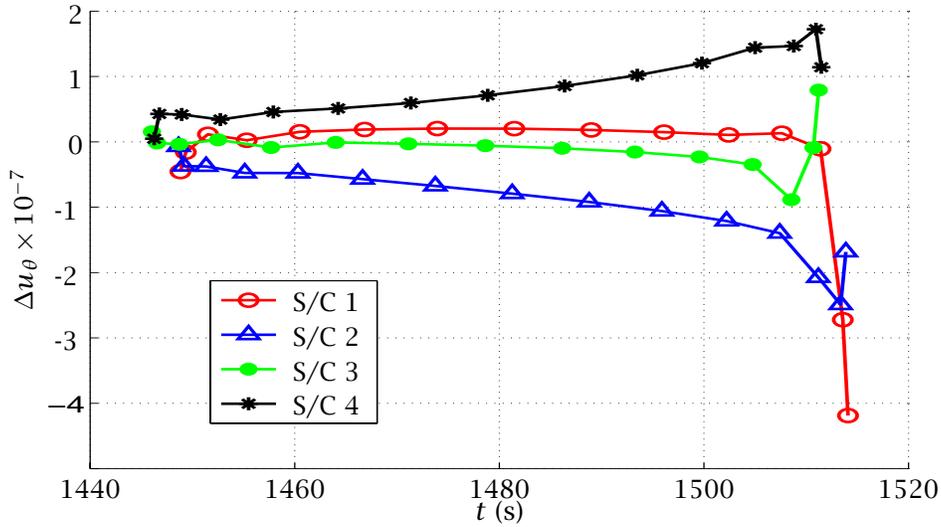
Figure 7: Transverse Error in Control for Phase 2 of the Basic Configuration Problem.
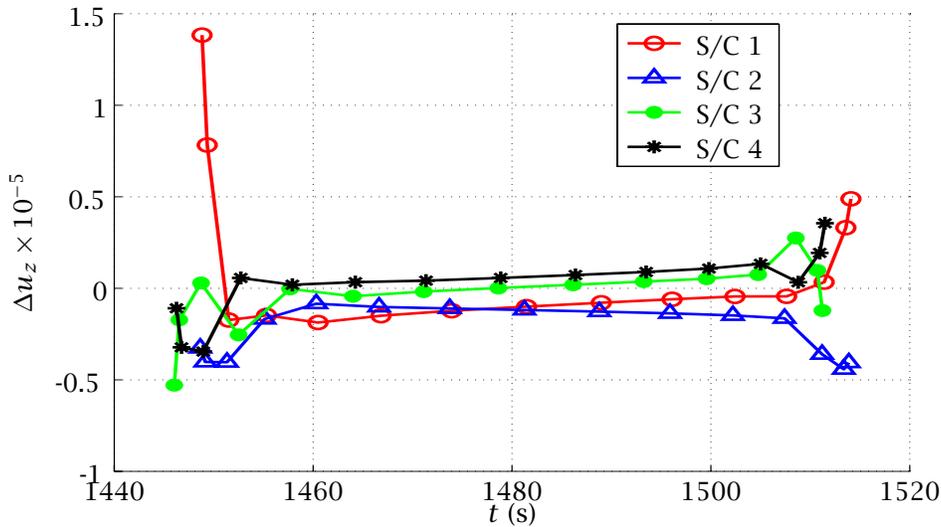
Figure 8: Normal Error in Control for Phase 2 of the Basic Configuration Problem.

12.2 Results for Extended Problem

The extended problem was formulated with four thrust phases and five coast phases. However, in the optimal solution the third and fourth burn phases were of zero duration. Furthermore, the second burn phase was of zero duration for all but one spacecraft. Consequently, three of the spacecraft had one-burn solutions, while one had a two-burn solution. Figs. 9-11 show the optimal control profile during this first burn phase for each component of control. The four arcs in each Figure represent the four spacecraft. Again, it can be seen that the control output from the NLP matches extremely well with the optimal control derived from the discrete first-order optimality conditions of the HBVP.

16
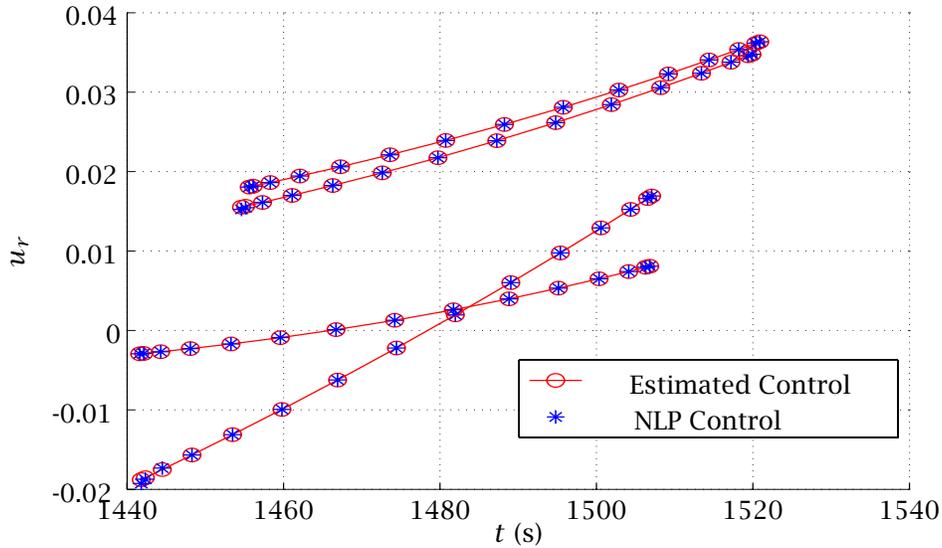
Figure 9: Radial Control Trajectory for Phase 2 of the Extended Configuration Problem.
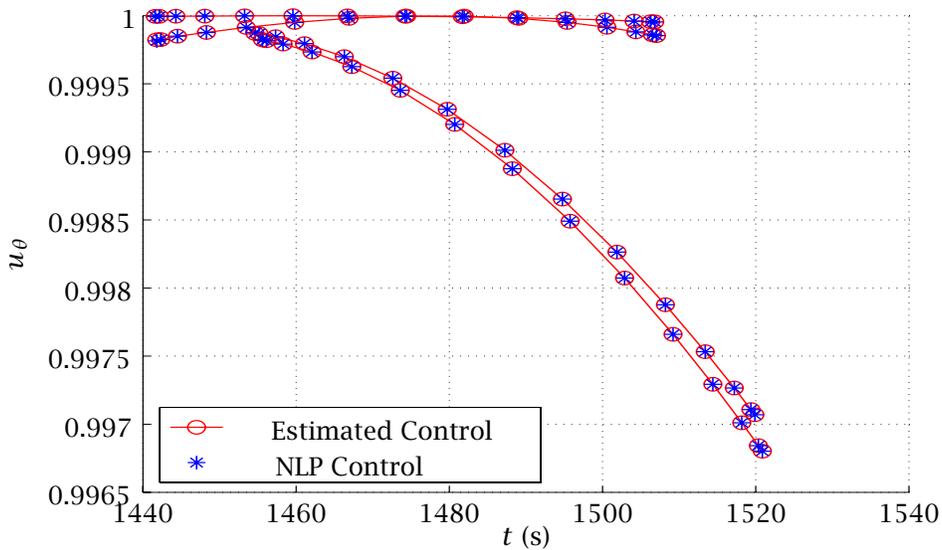
Figure 10: Transverse Control Trajectory for Phase 2 of the Extended Configuration Problem.

13 CONCLUSIONS

In this paper, the first-order optimality conditions obtained from the Gauss pseudospectral method were derived for a multiple-phase optimal control problem. These optimality conditions were compared with the optimality conditions obtained by discretizing the calculus of variations problem via the Gauss pseudospectral method. A relationship between the costates of both sets of conditions was then derived. Costate estimates from the Gauss pseudospectral method were then used to determine an estimate of the optimal control for a four spacecraft formation flying problem. It was found that the control obtained from the NLP was in excellent agreement with the control estimated by the discretized HBVP. This demonstrates the accuracy and usefulness of the Gauss pseudospectral method.
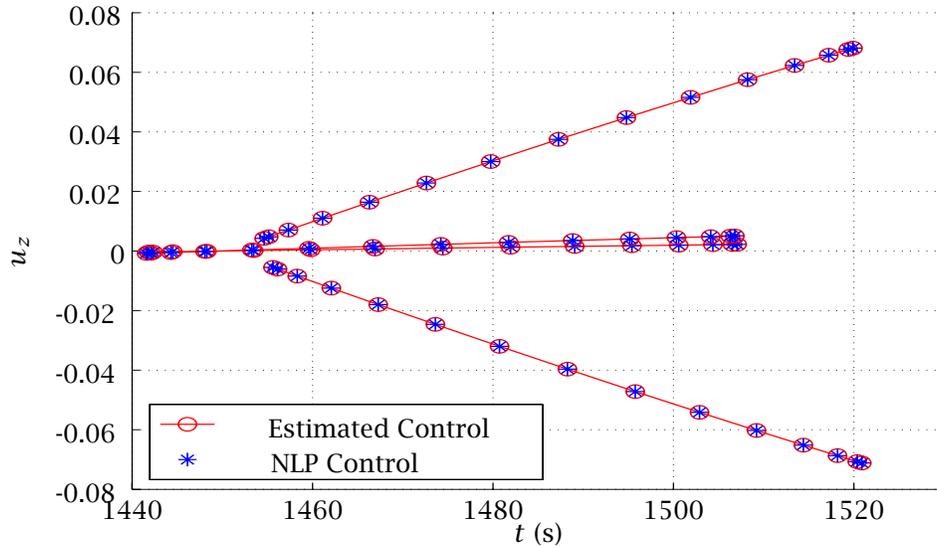
Figure 11: Normal Control Trajectory for Phase 2 of the Extended Configuration Problem.

DISCLAIMER

ACKNOWLEDGMENTS

REFERENCES

1. Betts, J. T., "Survey of Numerical Methods for Trajectory Optimization," *Journal of Guidance, Control, and Dynamics*, Vol. 21, No. 2, 1998, pp. 193–207.

2. Athans, M. and Falb, P. L., *Optimal Control*, McGraw-Hill, New York, 1966, pp. 284-351.

3. Betts, J. T.,, *Practical Methods for Optimal Control Using Nonlinear Programming*, Society for Industrial and Applied Mathematics Press, 2001.

4. Betts, J. T. and Frank, P. D., "A Sparse Nonlinear Optimization Algorithm," *Journal of Optimization Theory and Applications*, Vol. 82, pp. 519-541, 1994.

5. Gill, P. E., Murray, W., and Saunders, M. A., "SNOPT: An SQP Algorithm for Large-Scale Constrained Optimization," *SIAM Journal on Optimization*, Vol. 12, No. 4, 2002, pp. 979–1006.

6. Hargraves, C. R. and Paris, S. W., "Direct Trajectory Optimization Using Nonlinear Programming and Collocation," *Journal of Guidance, Control, and Dynamics*, Vol. 10, No. 4, 1987, pp. 338-342.

7. Williams, P. , "A Comparison of Differentiation and Integration Based Direct Transcription Methods", AAS/AIAA Space Flight Mechanics Conference, Copper Mountain, CO, Jan. 23-27, 2005. Paper AAS 05-128.

8. Vlases, W. G., Paris, S. W., Lajoie, R. M., Martens, M. J., and Hargraves, C. R., "Optimal Trajectories by Implicit Simulation," Boeing Aerospace and Electronics, Technical Report WRDC-TR-90-3056, Wright-Patterson Air Force Base, 1990.

9. Betts, J. T. and Huffman, W. P., "Sparse Optimal Control Software - SOCS," *Mathematics and Engineering Analysis Library Report*, MEA-LR-085, Boeing Information and Support Services, P. O. Box 3797, Seattle, WA, 98124-2297, 15 July 1997.

10. Well, K., *Graphical Environment for Simulation and Optimization*, Department of Optimization, Guidance, and Control, Stuttgart, Germany, 2002.

11. Von Stryk, O., "User's Guide for DIRCOL 2.1: A Direct Collocation Method for the Numerical Solution of Optimal Control Problems," Technische Universitat Darmstadt, 1999.

12. Ross, I. M. , "User's Manual for DIDO (Ver. PR.1β): A MATLAB Application Package for Solving Optimal Control Problems", *Technical Report 04-01.0*, February 2004.

13. Canuto, C., Hussaini, M.Y., Quarteroni, A., Zang, T.A., *Spectral Methods in Fluid Dynamics,* Springer-Verlag, New York, 1988.

14. Elnagar, G. , Kazemi, M. , Razzaghi, M. , "The Pseudospectral Legendre Method for Discretizing Optimal Control Problems," *IEEE Transactions on Automatic Control*, Vol. 40, No. 10, October 1995.

15. Fahroo, F. and Ross, I. M., "Co-state Estimation by a Legendre Pseudospectral Method," *Journal of Guidance, Control, and Dynamics*, Vol. 24, No. 2, March-April 2002, pp. 270-277.

16. Fahroo, F. and Ross, I. M. , "Direct Trajectory Optimization by a Chebyshev Pseudospectral Method," *Journal of Guidance, Control, and Dynamics*, Vol. 25, No. 1, January-February 2002, pp. 160–166.

17. Williams, P. , "Jacobi Pseudospectral Method for Solving Optimal Control Problems", *Journal of Guidance*, Vol. 27, No. 2,2003

18. Williams, P. , "Hermite-Legendre-Gauss-Lobatto Direct Transcription Methods in Trajectory Optimization", AAS/AIAA Space Flight Mechanics Conference, Copper Mountain, CO, Jan 23-27, 2005. Paper AAS 05-131.

19. Rao, A. V. and Clarke, K. A., "Performance Optimization of a Maneuvering Re-entry Vehicle Using a Legendre Pseudospectral Method," *2002 AIAA Atmospheric Flight Mechanics Conference*, AIAA Paper 2002-4885, Monterey, CA August 5–8, 2002.

20. Stanton, S. and Proulx, R., "Optimal Orbital Transfer Using a Legendre Pseudospectral Method," *AAS/AIAA Astrodynamics Specialist Conference*, AAS-03-574, Big Sky, Montana, August 3–7, 2003.

21. Ross, I., King, J., and Fahroo, F., "Designing Optimal Spacecraft Formations," *2002 AIAA/AAS Astrodynamics Specialist Conference*, AIAA Paper 2002-4635, Monterey, CA, August 5–8, 2002.

22. Ross, I. M. and D'Souza,C. , "Hybrid Optimal Control Framework for Mission Planning," *Journal of Guidance, Control, and Dynamics*, Vol. 28,No. 4,July-August 2005.

23. Benson, D., *A Gauss Pseudospectral Transcription for Optimal Control*, Ph.D. Dissertation, Department of Aeronautics and Astronautics, Massachusetts Institute of Technology, November 2004.

24. Huntington, G. T., and Rao, A. V., "Optimal Configuration of Spacecraft Formations via a Gauss Pseudospectral Method," *AAS Spaceflight Mechanics Meeting*, AAS 05-103, Copper Mountain, CO, Jan 2005.

25. Hull, D. G., *Optimal Control Theory for Applications*, Springer-Verlag, New York, 2003.

26. Kirk, D. E. , *Optimal Control Theory*, Prentice-Hall, Englewood Cliffs, NJ, 1970.

27. Battin, R. H., *An Introduction to the Mathematics and Methods of Astrodynamics*, AIAA Press, New York, 1987, pp. 490-493 and p. 119.

28. Wertz, J. R. and Larsen, W. J., *Space Mission Analysis and Design*, 3rd Edition, Microcosm Press, El Segundo, CA and Kluwer Academic Publishers, Dordrecht, The Netherlands, 1999, p. 694.

29. Gill, P.E., *Users Guide for SNOPT Version 7, A Fortran Package for Large-Scale Nonlinear Programming,* University of California, San Diego, La Jolla, CA, Sept 04.